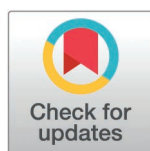


RESEARCH ARTICLE

Removal of hexavalent chromium from wastewater by chelating resin supported Fe/Cu bimetallic nanoparticles: Characterization, performance and mechanisms

Jialu Shi^{1,2,3}, Li Tang², Zhanhui Shen^{1,2,3}, Linan Deng¹, Xintong Liu¹

1 Henan Key Laboratory for Synergistic Prevention of Water and Soil Environmental Pollution, School of Geographic Sciences, Xinyang Normal University, Xinyang, China, **2** Key Laboratory for Yellow River and Huai River Water Environment and Pollution Control, Ministry of Education, Henan Key Laboratory for Environmental Pollution Control, School of Environment, Henan Normal University, Xinxiang, China, **3** State Key Laboratory of Pollution Control and Resource Reuse, School of the Environment, Nanjing University, Nanjing, China



OPEN ACCESS

Citation: Shi J, Tang L, Shen Z, Deng L, Liu X (2025) Removal of hexavalent chromium from wastewater by chelating resin supported Fe/Cu bimetallic nanoparticles: Characterization, performance and mechanisms. PLoS ONE 20(3): e0311898. <https://doi.org/10.1371/journal.pone.0311898>

Editor: Anil Kumar Reddy Police, Konkuk University - Seoul Campus: Konkuk University, KOREA, REPUBLIC OF

Received: October 13, 2024

Accepted: January 10, 2025

Published: March 18, 2025

Copyright: © 2025 Shi et al. This is an open access article distributed under the terms of the [Creative Commons Attribution License](https://creativecommons.org/licenses/by/4.0/), which permits unrestricted use, distribution, and reproduction in any medium, provided the original author and source are credited.

Data availability statement: All relevant data are within the paper and its [Supporting Information](#) files.

Funding: National Natural Science Foundation of China (No. 21407043) and College Student Research Fund Project of Xinyang Normal University (2024-DXS-111). The funders had

Abstract

In this work, Bimetallic Fe/Cu nanoparticles were successfully stabilized by chelating resin, which was specifically employed for the remediation of hexavalent chromium contaminated wastewater. Based on the characterization results, it was observed that the Fe/Cu bimetallic nanoparticles were uniformly and well distributed on the surface of the resin DOW M4195. The results demonstrated that the supported bimetallic Fe/Cu nanoparticles exhibited an excellent performance for Cr(VI) removal efficiency, reaching up to 99.4%. A series of factors, including initial pH, initial concentration of Cr(VI), co-exciting ions and humic acid were systematically evaluated to ascertain their respective impacts on Cr(VI) removal. The kinetics study followed intra-particle diffusion model demonstrated that both the adsorption and diffusion processes of Cr(VI) by the DOW M4195 resin played an important role in the overall removal of Cr(VI). The analytical results derived from XPS spectra at specific reaction times revealed the underlying removal mechanism of Cr(VI): Cr(VI) was adsorbed onto M-Fe/Cu due to the rich porous structure of the chelating resin DOW M4195. Additionally, the presence of the second metal, Cu, was found to significantly enhance the reduction performance of Fe⁰ and Fe(II) during the Cr(VI) removal process. The Cr(VI) removal mechanism was determined to involve a combination of physical adsorption, redox reactions and co-precipitation.

1. Introduction

Hexavalent chromium (Cr(VI)) is a typical toxic heavy metal ion that exists widely in industrial production processes such as processing of chromium ore, chemical manufacturing and electroplating [1]. The large amount of Cr(VI) containing wastewater and waste residue has led to serious Cr(VI) pollution in China's natural water bodies. The methods to remove Cr(VI) include adsorption [2], ion exchange, membrane separation and so on. Although these methods are effective, there is a risk of releasing Cr(VI) into the environment.

important roles in investigation, methodology, data collection and analysis and preparation of the manuscript.

Competing interests: The authors have declared that no competing interests exist.

Chromium predominantly exists in two valence states in the environment, Cr(VI) and Cr(III) [3]. Cr(VI) exhibits high mobile and pronounced toxicity in the environment, which is easily adsorbed by humans. Excessive exposure to substances containing Cr(VI) can substantially augment the cancer risk in humans. However, Cr(III) displays relatively weak migration and toxicity [4]. It is prone to hydrolysis in aqueous solution as the form of precipitates ($\text{Cr}(\text{OH})_3$ and Cr_2O_3) under alkaline or weakly acidic conditions [1]. Moreover, Cr(III) is also a necessary micro-precious element in the process of human metabolism [5]. Therefore, the conversion of highly toxic Cr(VI) into weakly toxic Cr(III) is one of the most effective approaches for controlling Cr(VI) pollution in water.

In recent years, nanoscale zero-valent iron (nZVI), which has high reducibility, environmental friendliness, strong absorption, low cost and easy to obtain [6], can achieve the reduction and fixation of Cr(VI) [7–9]. However, nZVI particles are susceptible to oxidize and agglomerate. The oxide layer of zero-valent iron can hinder the transport of electrons in the iron core, resulting in low activity of zero-valent iron. Many methods have been explored to enhance the activity of Fe^0 , including coupling Fe^0 with magnetic field [10], combining Fe^0 with strong oxidizer like H_2O_2 and persulfate [11, 12], as well as doping other metal elements onto the surface of Fe^0 . Among these methods, researchers have shown that doping an additional metal material on the surface of Fe^0 has shown significant advantages, including simple preparation, low cost and high electron selectivity. Many kinds of metals are used for modifying nZVI, such as Fe/Ni [13], Fe/Cu [14], Fe/Pd [15], Fe/Au bimetallic and so on. Precious metals showed high efficiency for pollutant removal. However, the high cost of precious metals limits their application [16]. Copper, in particular, has been proven to promote the activity of zero-valent iron and is often used as an additional metal in combination with iron [17]. Compared with other bimetallic materials, Fe/Cu bimetallic nanoparticles has distinct properties. For instance, precious metal bimetallics such as Fe/Pd and Fe/Au, despite being effective in pollutant removal, are restricted by their high cost [13]. Fe/Cu bimetallic nanoparticles, on the other hand, present a more economical option without sacrificing reactivity. The potential between Fe^0 and Cu^0 (0.777 V), being higher than that between Fe^0 and Fe^{2+} (0.441 V) [18], expedites the corrosion of Fe^0 and thereby augments the reduction ability of the material.

Bimetallic nanoparticles are prone to agglomeration and oxidation during both the preparation and usage processes. Loading bimetallic nanoparticles on a carrier can effectively address the issue of agglomeration. Stabilizers such as carbon nanotubes (CNTs) [19], biochar [20], resin [21], carboxymethyl cellulose (CMC) [22] and grapheme [23] have been employed. In our prior study, the chelating resin was used as the carrier of metal catalyst, and the pyridine group on the resin could chelate with metal ions [24, 25]. The strong binding of the support to the M-NPs can enhance the stability of the M-NPs and ultimately improve their activity and service life. The porous characteristics of the resin material not only provides more sites for the loading of metal particles, but also provides favorable conditions for the diffusion of pollutants into the resin. The combination of Fe/Cu bimetallic nanoparticles and chelating resin has not been extensively studied, and this combination is expected to synergistically enhance the performance for Cr(VI) removal.

Many studies have investigated the mechanism of Cr(VI) removal [16, 18, 26]. Nevertheless, the proposed mechanism still requires verification. Further systematic research is needed to clarifying the actual role of Fe/Cu in the reduction of Cr(VI) and the reaction process of Cr(VI). It is crucial for the further advancements in Fe-based decontamination technologies. In this study, through XPS analysis during specific reaction times, a more detailed reaction mechanism will be revealed, especially focusing on the change of Fe/Cu chemical valence states, the role of Cu on contaminants and electron transfer, as well as the conversion of Cr(VI) to Cr(III) during the redox reaction, which have been neglected in previous studies.

The investigation of the reaction kinetics of the chelating resin supported Fe/Cu bimetallic nanoparticles for Cr(VI) removal will provide valuable insights for the optimization and application of this material in the future.

The aim of this study was to (1) prepare chelating resin supported Fe/Cu bimetallic nanoparticles for Cr(VI) removal; (2) reveal the reaction mechanism according to the XPS analysis during specific reaction times; (3) investigate the reaction kinetics of the chelating resin supported Fe/Cu bimetallic nanoparticles for Cr(VI) removal.

2. Materials and methods

2.1 Materials and reagents

All chemicals used in this study are of analytical grade and were applied as delivered without further purification, including ferric sulfate ($\text{Fe}_2(\text{SO}_4)_3$), copper chloride dehydrate ($\text{CuCl}_2 \cdot 2\text{H}_2\text{O}$), potassium chromate (K_2CrO_4), ethyl alcohol, sodium borohydride (NaBH_4), sodium nitrate (NaNO_3), potassium dihydrogen phosphate (KH_2PO_4). The chelating resin DOW 3N (DOWEX™M4195) was purchased from Sigma Aldrich.

2.2 Synthesis of supported Fe^0 and Fe/Cu bimetallic nanoparticles

The supported Fe^0 nanoparticles and Fe/Cu bimetallic nanoparticles were prepared using a chemical reduction method with NaBH_4 as the reducing agent. Briefly, 0.5 g DOW M4195 was added into the dissolved solution containing 50 mL 0.2 mol/L Fe^{3+} solution and stirred for 30 min. Then, the resin spheres (DOW M4195- Fe^{3+}) were washed several times with deionized water. Subsequently, 50 mL of a 4 wt.% NaBH_4 solution was dropped slowly to reduce immobilized Fe^{3+} to Fe^0 under an N_2 environment for 2 h at 20 °C. The obtained black spheres M-Fe were rinsed multiple times with deionized water.

The supported Fe/Cu bimetallic nanoparticles were prepared using a similar method as described above for M-Fe synthesis but with some modifications: instead of only adding the dissolved solution containing 0.2 mol/L Fe^{3+} , it also contained either 0.0066 mol/L, 0.01 mol/L or 0.02 mol/L Cu^{2+} (the molar ratio between Fe/Cu being respectively set at: 3:1, 2:1, 1:1, respectively). The obtained black spheres were briefly named as M-Fe/Cu-1, M-Fe/Cu-2 and M-Fe/Cu-3, respectively.

2.3 Characterization of synthesized nanoparticles

The morphologies of Fe and Fe/Cu nanoparticles and the elemental composition were obtained using the scanning electron microscopy with energy dispersive X-ray spectroscopy (SEM-EDS, SU8010, Hitachi High-Technologies, Japan). The size and surface morphology of Fe and Fe/Cu nanoparticles were characterized using high-resolution transmission electron microscope (HR-TEM, JEM-2100) at 200KV with a resolution of 0.23 nm. The XPS spectras of the Fe and Fe/Cu before and after reaction were determined by an X-ray photoelectron spectrometer (XPS, ESCALAB 250Xi, Thermo Fisher, USA). The amount of Fe and Cu loaded into DOW M4195 and the released total iron ions and Cu^{2+} ions concentrations were determined by inductively coupled plasma mass spectroscopy (ICP-MS, ELAN DRC-e, PerkinElmer, USA).

2.4 Batch experiments

Batch experiments of Cr(VI) removal by supported Fe and Fe/Cu nanoparticles were carried out in a conical flask with 200 mL 20 mg/L Cr(VI). A certain amount of composites with 0.5 g supports was added to investigate the activity of Fe and Fe/Cu nanoparticles. The conical flask

were agitated at 25 °C at 180 rpm. The initial of pH of Cr(VI) solution was adjusted using HCl or NaOH. The experiment was carried out under aerobic conditions. At specific time intervals, aqueous samples were taken out to determine the concentrations of Cr(VI) and total Cr after filtered through 0.45 µm millipore filters.

2.5 Analytical methods

Cr(VI) concentration was determined using 1, 5-diphenylcarbazide colorimetric spectrophotometric method by an UV-visible spectrophotometer at the wavelength of 540 nm. The total Cr concentration was analysed with atomic absorption spectrometry (AA700, PerkinElmer, USA).

$$\text{The concentration of Cr(III)} = C_{\text{total Cr}} - C_{\text{Cr(VI)}} \quad (1)$$

Where $C_{\text{total Cr}}$ is the total Cr concentration and $C_{\text{Cr(VI)}}$ is the Cr(VI) concentration.

3 Results and discussion

3.1 Reduction activity of M-Fe/Cu composites

The influence of Fe/Cu mass ratio on the removal efficiency of Cr(VI) was investigated and the results were presented in Fig 1. The performance of M-Fe in removing Cr(VI) was also investigated. The concentration of Cr(VI) was gradually declined as reaction time increased. The removal efficiency of Cr(VI) by M-Fe reached 64.6% at 6 h while the removal efficiency of Cr(VI) attained 96.4%, 99.4% and 99.4% at 3 h by M-Fe/Cu-1, M-Fe/Cu-2 and M-Fe/Cu-3, respectively. Significantly increased Cr(VI) removal rate was observed in M-Fe/Cu compared with M-Fe. The results showed that the incorporation of Cu could effectively improve the Cr(VI) removal performance of M-Fe. The reason of this phenomenon is generally considered that copper deposition can form galvanic battery and electron transfer layer [27, 28]. The removal efficiency of Cr(VI) improved slightly with the increasing of Cu coating (Fe/Cu molar ratio from 3:1 to 2:1). However, almost no difference in removal efficiency of Cr(VI) was observed when the Cu coating increased continuously (Fe/Cu molar ratio from 2:1 to 1:1). The best performance of M-Fe/Cu for Cr(VI) removal was M-Fe/Cu-2 and M-Fe/Cu-3.

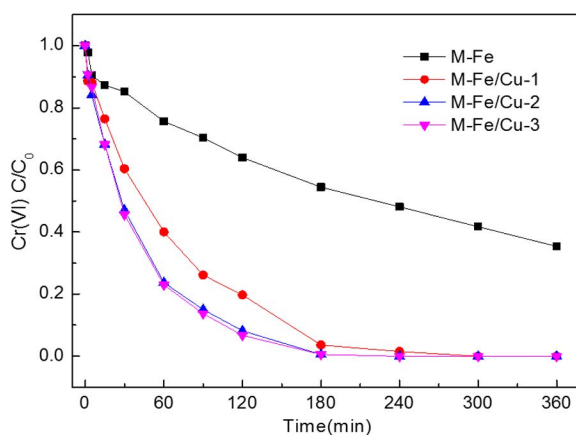


Fig 1. Cr(VI) removal performance by M-Fe and M-Fe/Cu with different Fe/Cu mass ratio (the initial concentration of Cr(VI): 20 mg/L, pH = 7, T = 25°C).

<https://doi.org/10.1371/journal.pone.0318180.g001>

Considering lower Cu coating of M-Fe/Cu-2, the subsequent batch experiments were carried out with M-Fe/Cu-2 (Fe/Cu molar ratio was 2:1).

3.2 Characterization of Fe/Cu bimetallic nanoparticles

The loading amount of Fe and Cu on resin was shown in [S1 Table](#). The Fe loading amount was 55.7 mg/g, and the Cu loading amount was 26.4 mg/g.

The surface morphology of M-Fe/Cu-2 was observed by SEM-EDS in [S1 Fig](#). The resin DOW M4195 was spherical with a diameter of approximately 0.6 mm. The EDS analysis was found that Fe and Cu was homogeneously distributed on the surface of the resin DOW M4195 ([S1 Fig \(c\) and \(d\)](#)). Furthermore, a large amount of C (49.2%) and N (5.5%) was detected due to the resin DOW M4195 structure. The large amount of O (28.8%) element may be contributed by the oxidation of Fe and Cu during the process of preparation and vacuum drying. In comparison with DOW M4195 ([S1 Fig \(e\)](#)), there are some small particles on the surface of the resin DOW M4195 for M-Fe/Cu-2 due to Fe/Cu loadings ([S1 Fig \(f\)](#)). The abundant pore structure on the chelating resin DOW M4195 can be seen from [S1 Fig \(e\) and \(f\)](#).

The BET surface area of DOW M4195 and M-Fe/Cu-2 was shown in [S2 Table](#). The results shown that after the loading of Fe and Cu on the chelating resin DOW M4195, the BET surface area was increased greatly. The pore-size distribution plot of DOW M4195 and M-Fe/Cu-2 before and after use was shown in [S2 Fig](#). In comparison with DOW M4195, the pore volume in the range of 2–15 nm was obviously increased after loading Fe/Cu bimetallic nanoparticles, and thereby the BET surface area was increased. However, the pore-size distribution hardly changed before and after the reaction.

The microscopic morphologies of Fe/Cu nanoparticles were investigated by TEM and the images were displayed in [S3 Fig](#). Black spherical Fe/Cu nanoparticles with a diameter of 5–10 nm were well-dispersed on the resin DOW M4195 which demonstrated that the resin DOW M4195 was a successful carrier helped to avoid the agglomeration of Fe/Cu nanoparticles.

[S4 Fig](#) presented the FTIR spectra of DOW M4195 and M-Fe/Cu-2 before and after reaction. In the FTIR spectrum of DOW M4195, four bands at 1589 cm^{-1} , 1569 cm^{-1} , 1433 cm^{-1} and 760 cm^{-1} were observed, which were associated with 2-picolylamine (the functional groups of the chelating resin DOW M4195). For the spectrum of M-Fe/Cu-2, the other new absorption peaks in the range of 2200–2400 cm^{-1} and at 3209 cm^{-1} could be ascribed to the bending vibration of B–O. This B–O was the residue left after the reduction of Fe/Cu with NaBH_4 . There was no significant change in the FTIR spectra of M-Fe/Cu-2 before and after the reaction of reducing Cr(VI).

XPS analysis were conducted to characterize the surface composition and chemical species of Fe/Cu bimetal nanoparticles and the results were shown in [Fig 2](#). The peaks of Fe 2p at 710 eV and 725 eV corresponded to Fe(II) and the peaks of Fe 2p at 712 eV and 727 eV corresponded to Fe(III). Meanwhile, the peak at 707 eV is the characteristic peak of Fe (0). The results of XPS patterns of Fe 2p revealed that the iron oxide existed on the surface of Fe (0). As shown in [Fig 2\(b\)](#), The Cu 2p peaks at 954.6 eV, 943.2 eV and 934.8 eV represent Cu(II). The intense peaks of Cu 2p at 952.3 eV and 932.5 eV were corresponding to Cu (0), which demonstrated that Cu(0) was successfully impregnated in the resin DOW M4195.

3.3 Factors affecting on the Cr(VI) reduction

3.3.1 Effect of initial pH on Cr(VI) reduction. The pH value play a critical role in Cr(VI) removal. The effect of initial pH on the removal of Cr(VI) by M-Fe/Cu-2 was presented in [Fig 3](#). The kinetic model was used to describe the kinetics of Cr(VI) reduction. The results

showed that Cr(VI) reduction kinetics accorded with the pseudo-first-order kinetic model. The pseudo-first-order kinetic model was shown below:

$$\frac{d[Cr(VI)]}{dt} = -K_{obs}[Cr(VI)] \quad (2)$$

$$\ln \left(\frac{[Cr(VI)]_0}{[Cr(VI)]_t} \right) = K_{obs}t \quad (3)$$

Where $[Cr(VI)]_t$ is the concentration of Cr(VI) (mg L^{-1}) at time t , $[Cr(VI)]_0$ is the initial concentration of Cr(VI) (mg L^{-1}), k_{obs} is the observed first-order rate constant (min^{-1}).

The results showed that the initial pH had a significant impact on Cr(VI) removal. M-Fe/Cu-2 has a higher removal efficiency at lower pH. The removal efficiency of Cr(VI) declined slightly as the initial pH value increased from 3 to 9. However, with the increasing of initial pH from 9 to 11, the decrease amplitude of Cr(VI) removal efficiency was greater. The k_{obs} was also decreased as the initial pH increased. The results indicated that the reduction process of

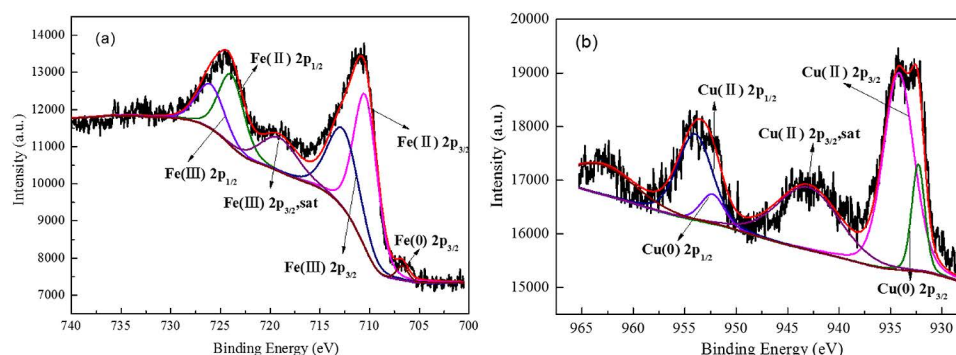


Fig 2. The XPS patterns of M-Fe/Cu-2: (a) Fe 2p and (b) Cu 2p.

<https://doi.org/10.1371/journal.pone.0318180.g002>

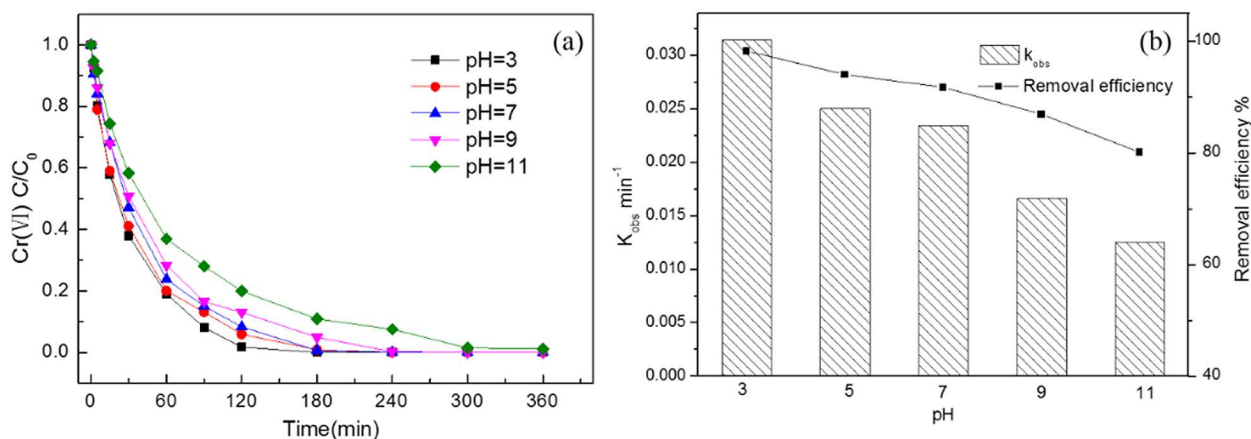
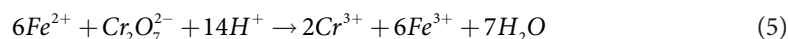
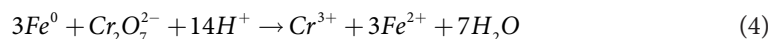


Fig 3. The effect of initial pH on the removal of Cr(VI) (a); the k_{obs} and the removal efficiency at 2 h (b) (the initial concentration was 20 mg/L Cr(VI), $T = 25^\circ\text{C}$).

<https://doi.org/10.1371/journal.pone.0318180.g003>

Cr(VI) was highly dependent on the initial pH, and the acidic conditions were favorable for the removal of Cr(VI).

S5 Fig showed the pH_{pzc} diagram of M-Fe/Cu-2. It can be seen from the figure that the pH_{pzc} of M-Fe/Cu-2 is approximately 7.8. When the pH of the solution is greater than 7.8, the surface potential of the material is negative, which is not conducive to the adsorption and diffusion of Cr(VI). Therefore, the removal efficiency and rate of Cr(VI) decrease under the conditions of pH 9 and 11. Conversely, when the pH of the solution is less than 7.8, the surface potential of the material is positive, which is conducive to the adsorption and diffusion of Cr(VI) and thus beneficial for the removal of hexavalent chromium.



Eqs. (4)–(5) showed that all the reactions of hexavalent chromium reduction by Fe/Cu nanoparticles consumed H^+ . This explained the reason why acidic conditions were favorable for the removal of Cr(VI). In addition, high pH values may lead to a passivation layer on the surface of Fe/Cu nanoparticles, which inhibited the reduction of Cr(VI).

3.3.2 Effect of initial concentration of Cr(VI) on Cr(VI) reduction. The effect of initial concentration on the removal of Cr(VI) by M-Fe/Cu-2 was shown in Fig 4. It was obvious that the removal efficiency of Cr(VI) declined slowly with the increase of the initial Cr(VI) concentration. Approximately 100% of Cr(VI) was eliminated within the first 3 h of the reaction when the initial Cr(VI) concentration was 10 or 20 mg/L. However, the removal efficiency was decreased when the initial Cr(VI) concentration increased to 30 or 40 mg/L. Similar to our results, Alessio Siciliano et al. also observed a slower Cr(VI) reduction with the increase of initial Cr(VI) concentration [29]. The decrease of removal efficiency may be ascribed to the coverage of excess Cr on the active sites of Fe/Cu nanoparticles. Moreover, the enhanced passivation of Fe/Cu nanoparticles at higher initial concentrations may also contribute to the lower efficiency. The reaction kinetics followed a first-order kinetic law with correlation coefficients R^2 ranging between 0.928 and 0.989.

3.3.3 Effect of co-exciting ions and HA on Cr(VI) reduction. This study investigated the effect of co-exciting ions (NO_3^- , HCO_3^- , SO_4^{2-} , Mg^{2+} and Ca^{2+}) and humic acid (HA) on Cr(VI) reduction by M-Fe/Cu-2. The results were shown in S6 Fig and S3 Table. The results indicated

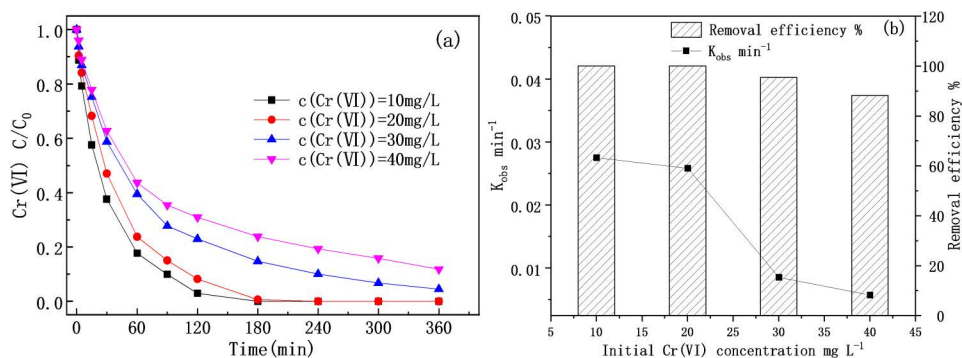


Fig 4. The effect of initial Cr(VI) concentration for the Cr(VI) reduction: the removal efficiency at 2 h (a) and the k_{obs} (b) (pH = 7, T = 25°C).

<https://doi.org/10.1371/journal.pone.0318180.g004>

that the co-existing anions such as NO_3^- , HCO_3^- , SO_4^{2-} had obvious inhibitory effect on the reduction of Cr(VI). This phenomenon mainly because the co-existing anions can react with Fe/Cu bimetallic nanoparticles or be adsorbed onto the surface of Fe/Cu oxides. It may also be attributed to their ability to compete with Cr(VI) for the active site on the surface of M-Fe/Cu-2 composite [30]. Moreover, with the increase of the co-existing anions concentration, the Cr(VI) removal rate decreased obviously. In contrast, in the presence of co-existing cations Mg^{2+} and Ca^{2+} , a different phenomenon was observed. The co-existing cations did not inhibit the removal of Cr(VI). Almost no change was observed in the removal of Cr(VI) in presence of Ca^{2+} . Furthermore, Mg^{2+} promoted the removal of Cr(VI) slightly. This is consistent with previous research results [31]. HA had obvious inhibitory effect on the removal of Cr(VI). The removal efficiency of Cr(VI) and K_{obs} decreased with the increasing concentration of HA. This was mainly because HA can be adsorbed onto the surface of the Fe/Cu nanoparticles and occupied the active sites [32].

3.4 Kinetic studies for Cr(VI) removal

Due to the porous structure of M4195 resin, the diffusion process of Cr(VI) may significantly impact the removal of Cr(VI). To understand the rate-determining step in this process, the intra-particle diffusion model was introduced.

The intra-particle diffusion model can be expressed by the following equation:

$$q_t = k_p t^{0.5} + C \quad (6)$$

Where, k_p is the diffusion rate constant ($\text{mg g}^{-1} \text{min}^{-0.5}$); q_t is the adsorption amount of Cr(VI) by the composite material at different reaction time t (mg/g); C is the parameter of intra-particle diffusion model (mg/g).

The resulting fitted curve was shown in [S7 Fig](#). The adsorption process of Cr(VI) by M-Fe/Cu-2 involved migration from the outer surface to the inner surface of the composite, which could be partitioned into three stages. The first stage is characterized by surface diffusion stage of Cr(VI). In this stage, Cr(VI) diffused from solution onto the surface of M-Fe/Cu-2. Due to a large number of active sites on the surface of the material, rapid Cr(VI) adsorption occurred with a high diffusion rate constant k_{p1} . The second stage was the intra-particle internal diffusion, as adsorbed Cr(VI) gradually diffused from the surface of the material towards the interior pores of the material. Simultaneously, nZVI played an important role in reducing Cr(VI). The third stage corresponded to an adsorption equilibrium phase. At this point, adsorption reached equilibrium due to low concentration of Cr(VI) in solution and the accumulation of Fe(III)-Cr(III) precipitates generated by the reaction leading to decreased availability of active site on M-Fe/Cu-2. Consequently, both the adsorption and diffusion of Cr(VI) by the DOW M4195 resin played an important role in the removal of Cr(VI).

3.5 Reaction mechanism

To investigate the adsorption of DOW M4195 resin for Cr(VI), Cr(VI) removal by the resin M4195 was investigated. As depicted in [S8 Fig](#), after 360 min, 23.1% removal efficiency was achieved without any detection of Cr(III). These results indicated that besides acting as support for Fe/Cu nanoparticles, M4195 resin also acted as an effective adsorbent for removing Cr(VI).

Furthermore, the activity of M-Fe/Cu-2 in the reduction of Cr(VI) was investigated in [S9 Fig](#). It was observed that the concentration of Cr(VI) in the solution decreased continually, while the concentration of Cr(III) increased gradually and reached its peak value at 60 min,

indicating the conversion of Cr(VI) to Cr(III). Simultaneously, the decrease in both Cr(III) and total chromium concentration suggested that adsorption or co-precipitation of Cr(VI) and Cr(III) may occur on the surface of M-Fe/Cu-2.

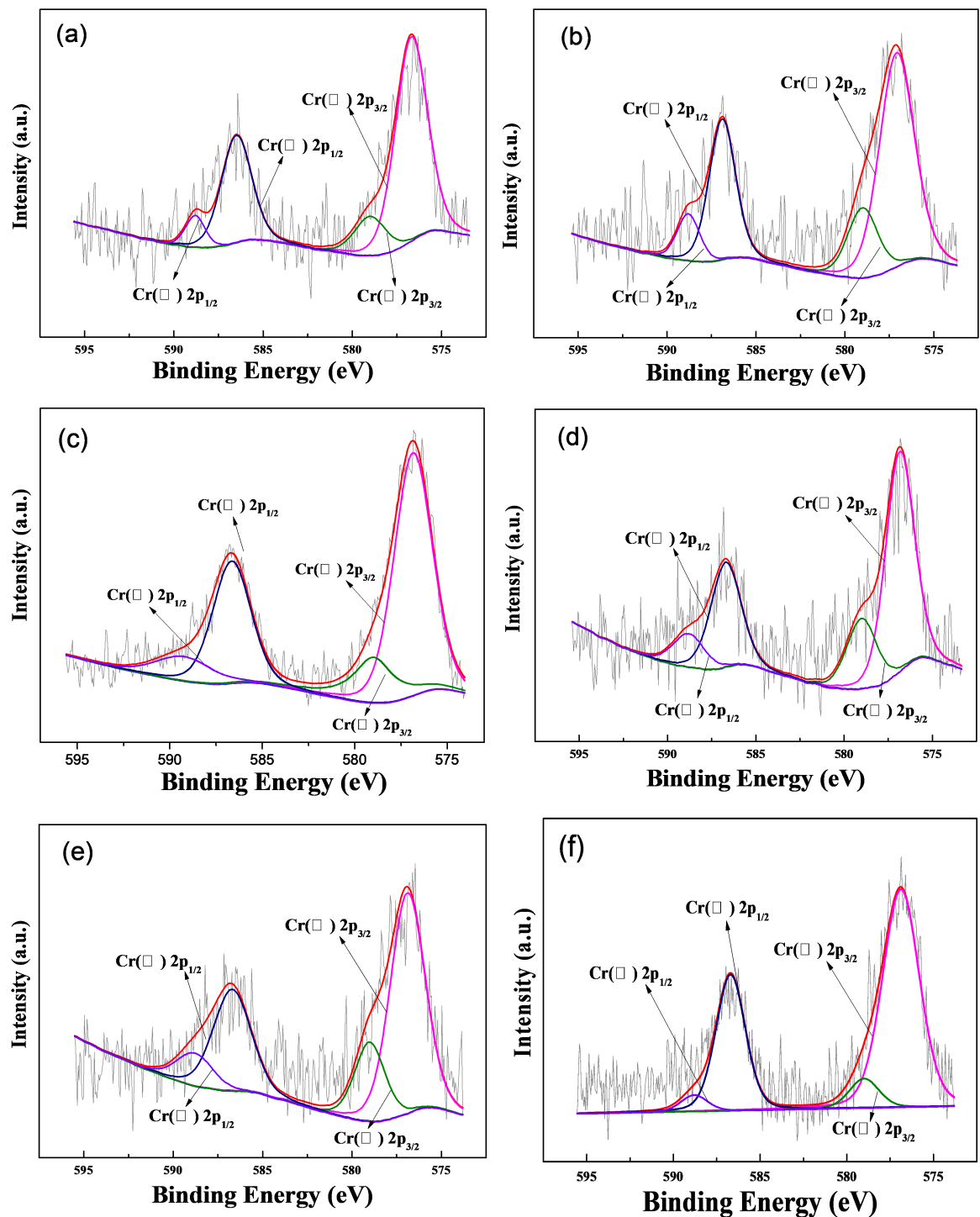


Fig 5. Cr 2p XPS analysis of M-Fe/Cu-2 after reaction for different time: (a) 5 min, (b) 15 min, (c) 60 min, (d) 90 min, (e) 180 min, (f) 360 min.

<https://doi.org/10.1371/journal.pone.0318180.g005>

In order to elucidate the reaction mechanism of Cr(VI), Cr 2p XPS analysis was conducted on used M-Fe/Cu-2 (Fig 5 (f)). The XPS spectra of Cr 2p region revealed coexistence of both Cr(VI) and Cr(III) on the surface of M-Fe/Cu-2 due to the strong peaks observed at 576.9 eV and 586.7 eV for Cr(III), as well as at 579.0 eV and 588.8 eV for Cr(VI). The results indicated that adsorption played a crucial role in capturing Cr(VI) by chelating resin DOW M4195 (as illustrated in S8 Fig), followed by subsequent reduction of a fraction of the adsorbed Cr(VI) to Cr(III) due to the presence of Fe-Cu bimetallic nanoparticles.

The process of Cr(VI) reduction was further investigated through XPS analysis of M-Fe/Cu-2 at specific reaction time (Fig 5 and Fig 6 (c)). The results demonstrated an initial decrease followed by an increase in the proportion of Cr(III) during the redox reaction. Conversely, the proportion of Cr(VI) exhibited precisely the opposite trend. This phenomenon can be explained by the fact that, in the initial stage, Cr(VI) is primarily adsorbed on the surface of M-Fe/Cu-2 and quickly converted to Cr(III). During this stage, the adsorption rate of Cr(VI) is higher than the reduction rate, resulting in an elevation in Cr(VI) content and a diminution of Cr(III) content on the surface of M-Fe/Cu-2. With the progression of the reduction reaction, the concentration of Cr(VI) in the solution decreased rapidly, and the content of Cr(VI) adsorbed by M-Fe/Cu-2 also declined, simultaneously being converted to Cr(III). This finding was consistent with the results of intraparticle diffusion kinetic fitting. Therefore, in the later stages of the reaction, the content of Cr(III) gradually increased. The binding energies at 576.7 eV and 586.3 eV correspond to Cr(III) species such as Cr_2O_3 , $\text{Cr}(\text{OH})\text{O}$ and $\text{Cr}(\text{OH})_3$ [33], indicating that the generated Cr(III) was co-precipitated on the surface of M-Fe/Cu-2. The adsorption and co-precipitation processes lead to a reduction in the total chromium concentration in the solution. Therefore, it can be inferred that the mechanism of Cr(VI) reduction may involve adsorption, reduction and co-precipitation.

Compared to fresh M-Fe/Cu-2, the XPS spectra of Fe 2p showed that the Fe^0 peak disappeared in used M-Fe/Cu-2 after the removal process, demonstrating a transformation from Fe^0 to Fe(II) or Fe(III) during the process of Cr(VI) reduction. Significant differences were observed when comparing changes in peak area proportion before and after reaction (as shown in Fig 7 and Fig 6 (a)). The proportion of Fe^0 gradually decreased and completely disappeared within 15 minutes of the reaction. As the reaction advanced, the proportion of Fe(II) gradually declined while the proportion of Fe(III) increased. This indicated that both Fe^0 and Fe(II) can be used to reduce Cr(VI). During the reaction, Fe^0 was oxidized either to Fe(II) or/and Fe(III), and furthermore, Fe(II) was further oxidized to Fe(III).

The XPS spectra of Cu 2p showed no significant changes in position and intensity of Cu peaks before and after the reaction as shown in Fig 6 (b) and Fig 8. The results indicated that Cu did not directly reduce Cr(VI), but rather provided an active site for electron transfer, consistent with previous study [14].

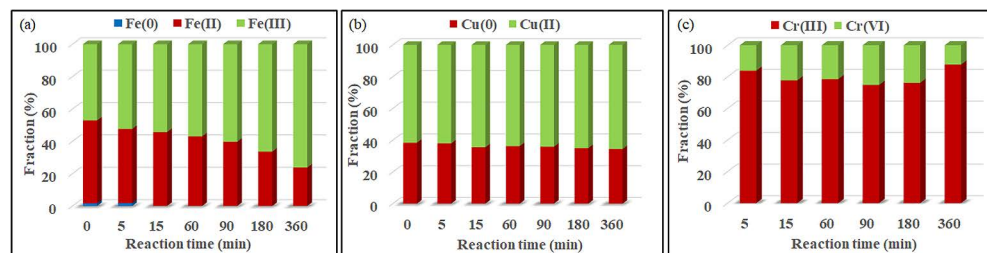


Fig 6. Fractions of Fe, Cu and Cr with different valence states in specific reaction time during the progress of Cr(VI) removal by M-Fe/Cu-2 according to the results of XPS spectra: (a) Fe, (b) Cu, (c) Cr.

<https://doi.org/10.1371/journal.pone.0318180.g006>

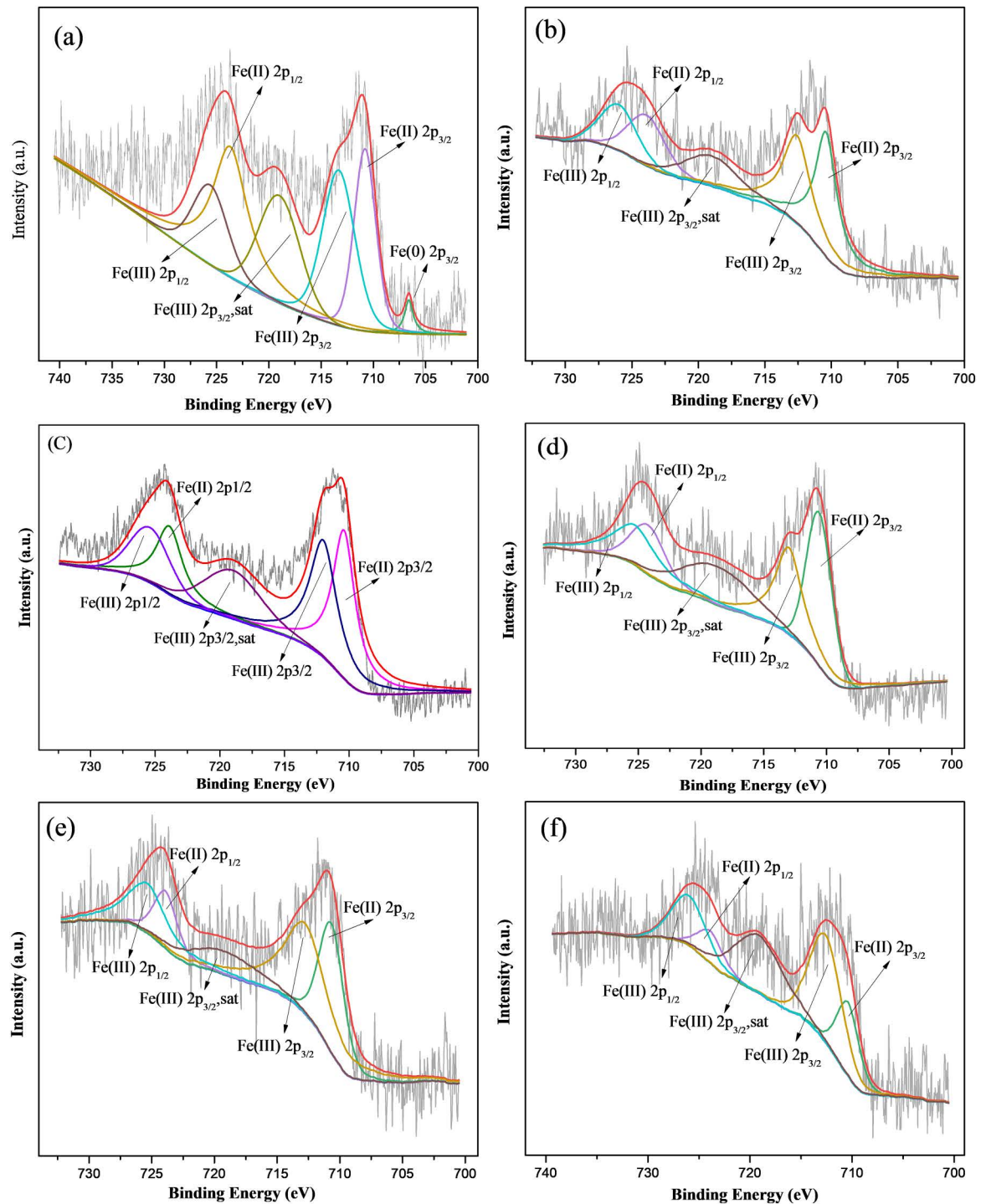


Fig 7. Fe 2p XPS analysis of M-Fe/Cu-2 after reaction for different time: (a) 5 min, (b) 15 min, (c) 60 min, (d) 90 min, (e) 180min, (f) 360 min.

<https://doi.org/10.1371/journal.pone.0318180.g007>

In conclusion, XPS analysis revealed that the removal of Cr(VI) by M-Fe/Cu-2 material mainly involved physical adsorption, redox reactions and co-precipitation mechanisms. The mechanism of Cr(VI) removal by M-Fe/Cu-2 was shown in Fig 9. The mechanism can be

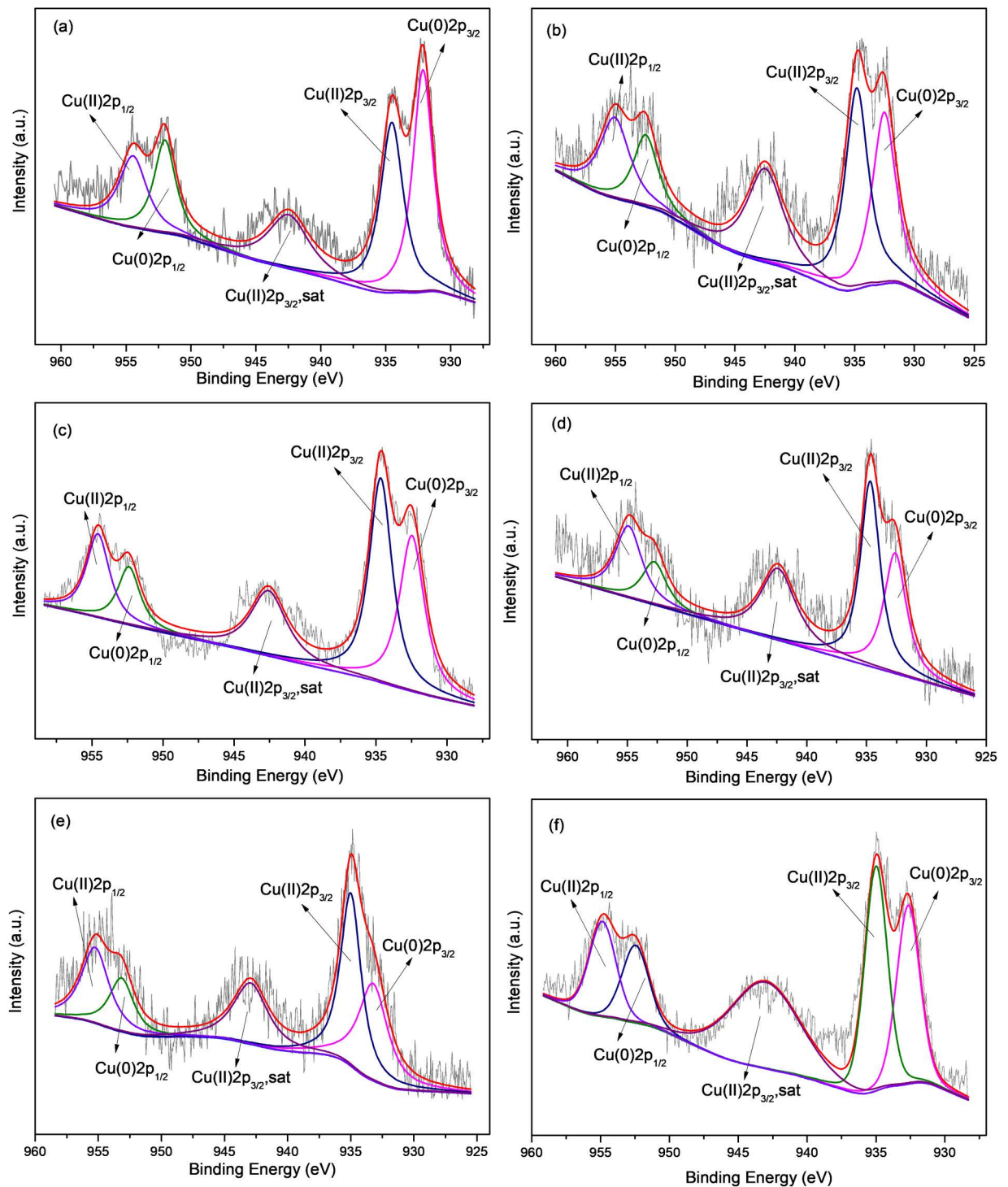
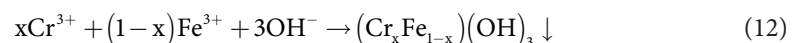
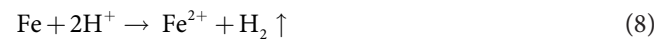
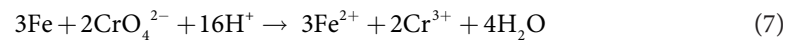


Fig 8. Cu 2p XPS analysis of M-Fe/Cu-2 after reaction for different time: (a) 5 min, (b) 15 min, (c) 60 min, (d) 90 min, (e) 180min, (f) 360 min.

<https://doi.org/10.1371/journal.pone.0318180.g008>

summarized as follows: in the initial phase of the reaction, when the concentration of Cr(VI) in the solution was relatively high, there is obvious adsorption onto M-Fe/Cu-2 material. Nano zero-valent iron on the material, catalyzed by Cu, reduced Cr(VI) to form Cr(III) and

Fe(II). The contact between nano zero-valent iron and liquid phase leads to formation of Fe(II) and H_2 . Subsequent reactions between generated Fe(II) and Cr(VI) result in formation of Cr(III) and Fe(III). As time elapsed, the pH value continuously ascended, prompting a gradual transformation from Cr(III) and Fe(III) to $Cr(OH)_3$, $Fe(OH)_3$ or Fe(III)-Cr(III) co-precipitation. The equation for this reaction mechanism for M-Fe/Cu-2 material in removing Cr(VI) are presented as follows:



4. Conclusions

In this study, the supported Fe/Cu nanoparticles were synthesized for the removal of Cr(VI). It was observed that Cu loading can significantly enhance the activity of nZVI in Cr(VI) removal. With the loading of Cu, the removal efficiency was increased from 64.6% to 99.4%. A number of factors, including initial pH, initial concentration of Cr(VI), co-exciting ions and humic acid influenced the performance of Fe/Cu bimetallic nanoparticles. A lower pH and lower initial concentration of Cr(VI) benefitted for Cr(VI) removal, while co-exciting ions and humic acid had adverse impacts. The kinetics study following intra-particle diffusion model demonstrated that the adsorption and diffusion of Cr(VI) by the DOW M4195 resin

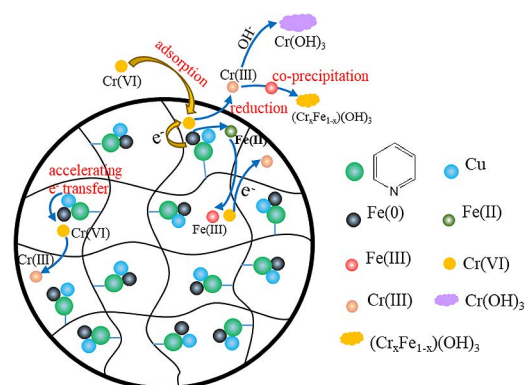


Fig 9. Schematic diagram of Cr(VI) removal by M-Fe/Cu-2.

<https://doi.org/10.1371/journal.pone.0318180.g009>

played an important role in the removal of Cr(VI). The XPS analysis of M-Fe/Cu-2 at specific reaction time was performed to elucidate the Cr(VI) removal mechanism. The results revealed that the Cr(VI) removal mechanism mainly involved physical adsorption, redox reactions and co-precipitation.

Supporting information

S1 Fig. SEM images and EDS spectrum of M-Fe/Cu-2.

(DOCX)

S2 Fig. The pore-size distribution plot of DOW M4195 and M-Fe/Cu-2 before and after use.

(DOCX)

S3 Fig. TEM images of M-Fe/Cu-2.

(DOCX)

S4 Fig. The FTIR spectra of DOW M4195 and M-Fe/Cu-2.

(DOCX)

S5 Fig. The pH_{Hzc} of M-Fe/Cu-2.

(DOCX)

S6 Fig. Effect of co-excited irons or HA on Cr(VI) reduction.

(DOCX)

S7 Fig. Internal diffusion model for Cr(VI) removal by M-Fe/Cu-2.

(DOCX)

S8 Fig. The adsorption of Cr(VI) by DOW M4195 resin ($M_{\text{resin}} = 0.5 \text{ g}$, the initial concentration of Cr(VI) = 20 mg/L, pH = 7).

(DOCX)

S9 Fig. The removal of Cr(VI) by M-Fe/Cu-2.

(DOCX)

S1 Table. The loading amount of Fe and Cu on resin.

(DOCX)

S2 Table. The BET surface area of DOW M4195 and M-Fe/Cu-2.

(DOCX)

S3 Table. Effect of co-excited irons or HA on Cr(VI) reduction: Kobs and R2.

(DOCX)

Author contributions

Data curation: Li Tang, Linan Deng, Xintong Liu.

Formal analysis: Li Tang.

Funding acquisition: Jialu Shi, Zhanhui shen, Linan Deng, Xintong Liu.

Investigation: Jialu Shi, Li Tang, Zhanhui shen, Linan Deng, Xintong Liu.

Methodology: Jialu Shi, Li Tang, Zhanhui shen, Linan Deng, Xintong Liu.

Writing – original draft: Jialu Shi, Zhanhui shen.

Writing – review & editing: Jialu Shi, Zhanhui shen.

References

1. Chen X, Li X, Xu D, Yang W, Bai S. Application of nanoscale zero-valent iron in hexavalent chromium-contaminated soil: A review. *Nanotechnol Rev*. 2020;9(1):736–50. <https://doi.org/10.1515/ntrev-2020-0059>
2. Pal CA, Choi J-S, Angaru GKR, Lingamdinne LP, Choi Y-L, Koduru JR, et al. Efficiency of Ppy-PA-pani and Ppy-PA composite adsorbents in Chromium(VI) removal from aqueous solution. *Chemosphere*. 2023;337:139323. <https://doi.org/10.1016/j.chemosphere.2023.139323> PMID: 37392794
3. Kadu BS, Chikate RC. nZVI based nanocomposites: Role of noble metal and clay support on chemisorptive removal of Cr(VI). *J Environ Chem Eng*. 2013;1(3):320–7. <https://doi.org/10.1016/j.jece.2013.05.011>
4. Ao M, Chen X, Deng T, Sun S, Tang Y, Morel JL, et al. Chromium biogeochemical behaviour in soil-plant systems and remediation strategies: A critical review. *J Hazard Mater*. 2022;424(Pt A):127233. <https://doi.org/10.1016/j.jhazmat.2021.127233> PMID: 34592592
5. Balmer J. Hexavalent chromium. *Workplace Health Saf*. 2018;66(11):564. <https://doi.org/10.1177/2165079918805775> PMID: 30340452
6. Di L, Chen X, Lu J, Zhou Y, Zhou Y. Removal of heavy metals in water using nano zero-valent iron composites: A review. *J Wat Process Eng*. 2023;53:103913. <https://doi.org/10.1016/j.jwpe.2023.103913>
7. Xie L, Chen Q, Liu Y, Ma Q, Zhang J, Tang C, et al. Enhanced remediation of Cr(VI)-contaminated soil by modified zero-valent iron with oxalic acid on biochar. *Sci Total Environ*. 2023;905:167399. <https://doi.org/10.1016/j.scitotenv.2023.167399> PMID: 37793443
8. Wang M, Chen Y, Zhang Y, Wei S, Zhao X, Zhao K, et al. Selective removal of Cr(VI) from solution by polyethyleneimine modified hydrochar loaded nanoscale zero-valent iron with high adsorption capacity. *Sep Purific Technol*. 2024;329:125150. <https://doi.org/10.1016/j.seppur.2023.125150>
9. Deng Y, Wang X, Lynch I, Guo Z, Zhang P, Wu L, et al. Homogeneous dispersion of amorphous nanoscale zero-valent iron supported on chlorella-derived biochar: In-situ synthesis and application mechanism for Cr(VI) removal over a wide pH range. *Sep Purific Technol*. 2024;330:125207. <https://doi.org/10.1016/j.seppur.2023.125207>
10. Cui YP, Huang Q, Cao JG, Dong W, Cui XX, Lu Y, et al. Nitrilotriacetic acid/Fe⁰/H₂O₂ system enhanced by magnetic field and visible light promoted DMP degradation and high-salt wastewater treatment. *Int J Environ Sci Technol*. 2024;21(15):9501–12. <https://doi.org/10.1007/s13762-024-05615-7>
11. Wang F, Gu Z, Hu Y, Li Q. Split dosing of H₂O₂ for enhancing recalcitrant organics removal from landfill leachate in the Fe⁰/H₂O₂ process: Degradation efficiency and mechanism. *Sep Purific Technol*. 2022;278.
12. Liu R, Yang J. Enhanced removal of sulfamethoxazole in soil by ball-milled Fe⁰-FeS@BC activated persulfate process. *J Environ Chem Eng*. 2023;11(5):110747. <https://doi.org/10.1016/j.jece.2023.110747>
13. Ruan X, Liu H, Ning X, Zhao D, Fan X. Screening for the action mechanisms of Fe and Ni in the reduction of Cr(VI) by Fe/Ni nanoparticles. *Sci Total Environ*. 2020;715:136822. <https://doi.org/10.1016/j.scitotenv.2020.136822> PMID: 32023522
14. Guo Y, Zhao Y, Yang T, Gong B, Chen B. Highly efficient nano-Fe/Cu bimetal-loaded mesoporous silica Fe/Cu-MCM-41 for the removal of Cr(VI): Kinetics, mechanism and performance. *J Hazard Mater*. 2021;418:126344. <https://doi.org/10.1016/j.jhazmat.2021.126344> PMID: 34130165
15. Wei X, Zhu N, Huang J, Kang N, Li F, Wu P, et al. Rapid and efficient reduction of chromate by novel Pd/Fe@biomass derived from *Enterococcus faecalis*. *Environ Res*. 2022;204(Pt A):112005. <https://doi.org/10.1016/j.envres.2021.112005> PMID: 34499894
16. Bashir MS, Ramzan N, Najam T, Abbas G, Gu X, Arif M, et al. Metallic nanoparticles for catalytic reduction of toxic hexavalent chromium from aqueous medium: A state-of-the-art review. *Sci Total Environ*. 2022;829:154475. <https://doi.org/10.1016/j.scitotenv.2022.154475> PMID: 35278543
17. Yao Y, Yin H, Zhang Y, Wei F, Hu H, Tang Y, et al. Fe, Cu-coordinated ZIF-derived bimetal encapsulated N-doped carbon nanotube for efficient remediation of various aqueous pollutants. *Chem Eng J*. 2021;426:131801. <https://doi.org/10.1016/j.cej.2021.131801>
18. Yuan Y, Zhou Z, Zhang X, Li X, Liu Y, Yang S, et al. Efficient reduction of hexavalent chromium with microscale Fe/Cu bimetal: Efficiency and the role of Cu. *Chin Chem Lett*. 2023;34(6):107932. <https://doi.org/10.1016/j.ccllet.2022.107932>
19. Yang Y, Liu M, You X, Li Y, Lin H, Chen JP. A novel bimetallic Fe-Cu-CNT catalyst for effective catalytic wet peroxide oxidation: reaction optimization and mechanism investigation. *Chem Eng J*. 2024;479:147320. <https://doi.org/10.1016/j.cej.2023.147320>

20. Wang H, Zhuang M, Shan L, Wu J, Quan G, Cui L, et al. Bimetallic FeNi nanoparticles immobilized by biomass-derived hierarchically porous carbon for efficient removal of Cr(VI) from aqueous solution. *J Hazard Mater.* 2022;423(Pt A):127098. <https://doi.org/10.1016/j.jhazmat.2021.127098> PMID: [34523485](https://pubmed.ncbi.nlm.nih.gov/34523485/)
21. Shen Z, Fang M, Tang L, Shi J, Wang W. Pd/Cu bimetallic nano-catalyst supported on anion exchange resin (A520E) for nitrate removal from water: High property and stability. *Environ Res.* 2024;241:117616. <https://doi.org/10.1016/j.envres.2023.117616> PMID: [37956750](https://pubmed.ncbi.nlm.nih.gov/37956750/)
22. Mondal A, Arora M, Kumar Dubey B, Mumford K. Comparative assessment of the characteristics and Cr(VI) removal activity of the bimetallic Fe/Cu nanoparticles pre- and post-coated with carboxymethyl cellulose. *Chem Eng J.* 2022;444:136343. <https://doi.org/10.1016/j.cej.2022.136343>
23. Hanyong L, Xin L, Daming Z, Guotao Z, Bo Y. Preparation of graphene supported Ni-Fe bimetallic nanocatalyst and its catalytic upgrading and viscosity reduction performance for heavy oil. *Geoenergy Science and Engineering.* 2023;227:211847. <https://doi.org/10.1016/j.geoen.2023.211847>
24. Shi J, Gao Y, Zang L, Shen Z, Peng G. Performance of Pd/Sn catalysts supported by chelating resin pre-storing reductant for nitrate reduction in actual water. *Environ Res.* 2021;201:111577. <https://doi.org/10.1016/j.envres.2021.111577> PMID: [34228952](https://pubmed.ncbi.nlm.nih.gov/34228952/)
25. Zang L, Shi J, Shen Z. Practical application of Pd-based bimetallic catalysts with enhanced selectivity supported by chelating resin for catalytic nitrate reduction in real water. *Nanotechnology.* 2023;34(39):10.1088/1361-6528/ace170. <https://doi.org/10.1088/1361-6528/ace170> PMID: [37356427](https://pubmed.ncbi.nlm.nih.gov/37356427/)
26. Li J, Fan M, Yuan Z, Liu F, Li M. One-Pot synthesis of lamellar Fe-Cu bimetal-decorated reduced graphene oxide and its enhanced removal of Cr(VI) from water. *Nanomaterials.* 2023;13.
27. Qu M, Chen H, Wang Y, Wang X, Tong X, Li S, Xu H. Improved performance and applicability of copper-iron bimetal by sulfidation for Cr(VI) removal. *Chemosphere.* 2021;281.
28. Hu C-Y, Lo S-L, Liou Y-H, Hsu Y-W, Shih K, Lin C-J. Hexavalent chromium removal from near natural water by copper-iron bimetallic particles. *Water Res.* 2010;44(10):3101–8. <https://doi.org/10.1016/j.watres.2010.02.037> PMID: [20350740](https://pubmed.ncbi.nlm.nih.gov/20350740/)
29. Siciliano A, Curcio GM, Limonti C. Hexavalent chromium reduction by zero-valent magnesium particles in column systems. *J Environ Manage.* 2021;293:112905. <https://doi.org/10.1016/j.jenvman.2021.112905> PMID: [34089953](https://pubmed.ncbi.nlm.nih.gov/34089953/)
30. Angaru GKR, Choi Y-L, Lingamdinne LP, Choi J-S, Kim D-S, Koduru JR, et al. Facile synthesis of economical feasible fly ash-based zeolite-supported nano zerovalent iron and nickel bimetallic composite for the potential removal of heavy metals from industrial effluents. *Chemosphere.* 2021;267:128889. <https://doi.org/10.1016/j.chemosphere.2020.128889> PMID: [33187656](https://pubmed.ncbi.nlm.nih.gov/33187656/)
31. Li J, Fan M, Li M, Liu X. Cr(VI) removal from groundwater using double surfactant-modified nanoscale zero-valent iron (nZVI): Effects of materials in different status. *Sci Total Environ.* 2020;717:137112. <https://doi.org/10.1016/j.scitotenv.2020.137112> PMID: [32084682](https://pubmed.ncbi.nlm.nih.gov/32084682/)
32. Wang Y, Gong Y, Lin N, Yu L, Du B, Zhang X. Enhanced removal of Cr(VI) from aqueous solution by stabilized nanoscale zero valent iron and copper bimetal intercalated montmorillonite. *J Colloid Interface Sci.* 2022;606(Pt 2):941–52. <https://doi.org/10.1016/j.jcis.2021.08.075> PMID: [34487941](https://pubmed.ncbi.nlm.nih.gov/34487941/)
33. Jia T, Zhang B, Huang L, Wang S, Xu C. Enhanced sequestration of Cr(VI) by copper doped sulfidated zerovalent iron (SZVI-Cu): Characterization, performance, and mechanisms. *Chem Eng J.* 2019;366:200–7. <https://doi.org/10.1016/j.cej.2019.02.058>